J MATER SCI 41 (2006) 423–430

Permeability and high temperature strength of porous mullite-alumina ceramics for hot gas filtration

B. A. LATELLA*, L. HENKEL†, E. G. MEHRTENS
Materials and Engineering Science, Australian Nuclear Science and Technology Organisation, Private Mail Bag 1, Menai, New South Wales 2234, Australia
E-mail: bal@ansto.gov.au

Published online: 12 January 2006

The gas permeability and mechanical properties of mullite-alumina ceramics for potential use as filters in hot gas separation environments are examined. The mullite-alumina ceramics with different levels of induced porosity and pores sizes were fabricated by slip casting and characterised in terms of microstructure and strength properties at ambient and elevated temperatures. Permeability to nitrogen gas flow of the porous structures at ambient temperature was investigated over a range of flow velocities to quantify and assess the permeability. The strength at high temperatures is equivalent to ambient data signifying no discernible degradation. Nitrogen gas permeability tests reveal dramatic reductions in the pressure drop–gas velocity curves with increasing porosity. It is shown that the gas permeability increases with the level of porosity and pore size, with maximum Darcian permeability constant of $k = 2.5 \times 10^{-14}$ m^2 for a porosity of 71%.

1. Introduction

Ceramic filters are widely used in locations where hot gas cleaning is crucial particularly coal combustion and gasification in the power generation industry [1–3]. The "dirty" gases emitted require adequate filtration to minimise particulate waste to a gas stream and also the atmosphere and surrounding environment. Leading ceramic filter candidates for high temperature use are cordierite, mullite, alumina and silicon carbide. The design requirements for these ceramic filters, whose main function is removal of fine particles at elevated temperature, are high porosity (≈50 to 80%), adequate strength (generally exceeding 5 MPa at the operating temperature—based purely on the gas pressure used), erosion resistance, thermal shock resistance and decent flow or permeability characteristics. Accordingly, the suitability of materials for these types of filter applications depends critically on the microstructure and the associated mechanical and thermal properties [4]. Work has demonstrated that the performance of porous ceramics is controlled by the pore volume fraction, pore size and shape and the matrix grain size and intergrain bonding [5–7]. At the same time, it is well recognised that porosity is an important microstructural defect affecting the mechanical properties and wear susceptibility [8–11]. It is in this context that the gas permeability and strength response of these materials requires serious consideration.

In service, these filters are subjected to repeated impacts from fine particles, generally 8 μm or greater travelling at velocities of between 2 and 5 cm/s in a gas stream at temperatures normally ranging from 400 to 1000°C. So the filter element must be able to withstand the contact of particles, the sudden temperature increase at the face of the filter and the pressure differential due to the gas. Furthermore particles from the gas stream may form a cake at the surface of the filter on the inlet side or become embedded in the pores of the filter, which can reduce the efficiency of operation quite considerably [12, 13]. To circumvent this potential problem these filters are cleaned periodically (i.e. in a pulsing sequence) during operation by backfilling with compressed air, which can remove caking from the surface and unclog the pores. But again thermal shock due to the sudden temperature gradient could adversely affect filter lifetime.

Mullite is a promising candidate for use in hot gas filter applications as it can be processed economically but more importantly it possesses several key beneficial attributes

*Author to whom all correspondence should be addressed.
† : Year-in-Industry student from the Department of Production Engineering, University of Bremen, Bibliothekstraße 1, Bremen 28359, Germany.

0022-2461
DOI: 10.1007/s10853-005-2654-8

that are important in operation, namely low thermal expansion, good thermal shock and corrosion resistance and high temperature mechanical stability [14]. The high temperature strength of ceramic filter elements is of considerable practical importance as they are subjected to prolonged use at high temperature. To address this issue studies are being conducted in our laboratory to investigate processing routes in a range of alumina- and mullite-based ceramics with different degrees of porosity, using readily available raw materials, with the intent of optimising properties [7, 9, 11, 15]. Consequently, improving service performance, reliability and lifetime of these ceramic filters is paramount to minimise the large maintenance costs and downtime incurred due to a failure of a filter element and the potential contamination to the atmosphere and surrounding environment.

In this paper we investigate the gas permeability and mechanical properties of mullite-alumina ceramics with varying levels of porosity. The materials were characterised in terms of microstructure and strength properties at ambient and elevated temperatures. Further, the room temperature gas permeability of the porous structures was investigated at a range of flow velocities. The implications of microstructural changes on the gas permeability and strength are considered.

2. Experimental

2.1. Processing and characterisation

Commercially available alumina (α-Al_2O_3, $\approx$1 μm mean particle size, Reynolds 99.7% purity) and silica (Nyacol-1440, median particle size = 14 nm) powders were used as raw materials. The powders were mixed in proportions of 75 wt% ($\approx$63 vol%) alumina to 25 wt% ($\approx$37 vol%) silica in water containing a small amount of deflocculant (3 wt%, Dispex A40, Allied Colloids) to aid dispersion. This composition was deliberately chosen so that an excess of alumina (yielding $\approx$15% from batch composition calculations) remained after the silica reacted with alumina to form mullite, $3Al_2O_3{\cdot}2SiO_2$ ($\approx$85%). Individual slurry batches were prepared with about 20 vol% solids loading and these were mixed by ball milling using alumina media in polyethylene containers for 24 h and then a further 2 h with differing amounts of a pore former agent (graphite powder, KS75, median particle size = 23 μm, TIMCAL Ltd., Switzerland). The graphite addition ranged from 0 to 60 vol%. The compositions are designated by the percentage of graphite addition, i.e., MA20G denotes 20% graphite to the mullite-alumina mixture. Examination of specific properties focussed on four compositions: MA0G, MA20G, MA40G and MA60G. The slurries were sieved through a 300 μm sieve to separate the alumina grinding media and then slip cast in split-plaster moulds to form disks of diameter 30 mm and thickness of 5 to 10 mm. The green samples were then sintered in air using a resistance-heated furnace. A heating rate of 60°C/h to 1200°C hold for 1 h then 300°C/h to 1540°C for 5 h dwell followed by a 300°C/h cooling rate to room temperature was used. The graphite is burned out at <1000°C during the heat up cycle as determined from differential thermal analysis (DTA) and thermogravimetric (TG) techniques as shown in Fig. 1.

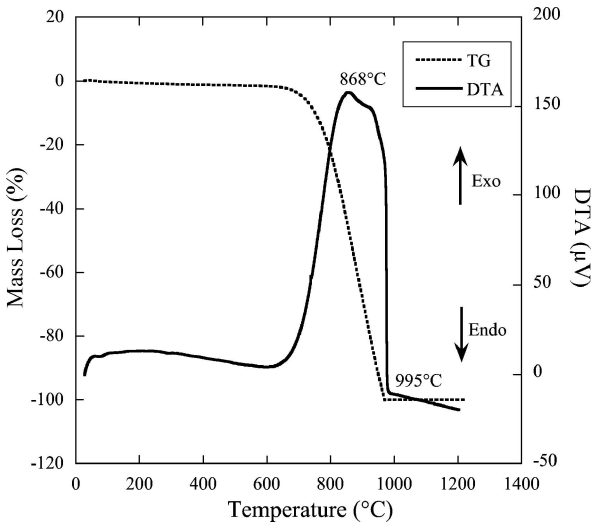

Figure 1 Differential thermal analysis (DTA) and thermogravimetric (TG) curves for the graphite powder on heating to 1200°C.

X-ray diffraction (XRD) was used to determine the phase composition of sintered specimens. Some sintered specimens were cut, ground and polished to a 1 μm finish using routine ceramographic techniques. These specimens were then sputtered coated with carbon for examination in an SEM (Jeol JSM-6400) to ascertain grain size and pore structure. Backscattered electron imaging along with qualitative energy dispersive spectroscopy (EDS) using a microanalysis system (Model Voyager, Noran Instruments) were used to identify alumina and mullite grains. The bulk density and apparent porosity of all the materials were measured using the Archimedes method, with deionised water as the immersion medium. Pore size distribution was determined from several SEM images taken from random areas of the specimens and using the public domain NIH image program (Scion Image 1.62c, US National Institutes of Health) to calculate pore size assuming an elliptical pore shape. The average pore size was then determined from all the pores counted for each material microstructure.

2.2. Mechanical properties

Hardness was evaluated from Vickers indentations on polished specimens at indentation loads of 5, 10 and 20 N. The lengths of residual impression diagonals from at least five indentations at each load were measured using a calibrated microscope. Hardness was evaluated as the load per contact area.

As-sintered disks were carefully ground to about 3 mm thickness using SiC paper. Young's modulus of selected specimens was determined using an impulse excitation

technique [16]. The strength of these specimens were then determined using a three-point biaxial flexure test on a universal testing machine (Instron 8562) at room temperature (≈20°C) with a loading rate of 10 μm/s. A flat circular WC punch with a contact diameter of 4 mm, on a three-point support 25.4 mm in diameter was employed. Strengths were calculated from the failure loads and specimens dimensions with a minimum of 5 disks broken in each instance [17].

For high temperature biaxial strength, specimens were placed on an alumina jig with 3 mm alumina balls as the supports in circumference (support diameter = 24 mm) and a flat alumina punch with the same contact area as the WC punch used for the ambient temperature measurements. A resistance-heated furnace rated to 1500°C attached to a servo-electric universal testing machine (Instron 8561) was used. Specimens were placed centrally in the jig that was held in place by thick alumina loading rods. Each test sample was then heated at 300°C/h to the designated temperature (800 or 1200°C) and held for 30 min to equilibrate prior to loading to failure at 10 μm/s. The strength values were computed as described previously with five disks broken in each instance.

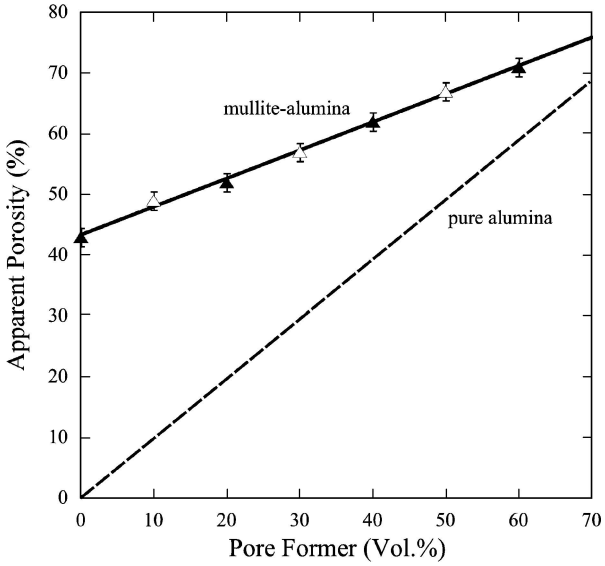

Figure 2 Apparent porosity as a function of graphite addition for all the mullite-alumina samples fabricated. Filled symbols pertain to samples described in Table I. Solid line is the least squares fit to the mullite-alumina data and for comparison the dashed line is from measurements on pure alumina [7].

2.3. Gas permeability

Gas permeability of the materials was studied using a permeability apparatus based on the ASTM standard [18]. Nitrogen gas was passed through the chamber in which the sample is tightly held in a central hole of a thick polyurethane holder and two sensors measured the pressure in the inlet and outlet gas line at ambient temperature. A flow meter was used to determine the gas flow, Q, in litres per minute.

The permeability of a porous material is governed by Darcy's law [19, 20]:

$$\frac{\Delta P}{L} = \frac{\mu}{k} v \tag{1}$$

where ΔP is the pressure drop, L is the thickness of the material, μ is the viscosity of the gas, v is the fluid velocity and k is the specific permeability. The fluid velocity is obtained from the flow, Q, divided by the cross-sectional area of the sample. In the case of compressible fluids (i.e., nitrogen gas) flowing through a solid porous medium the specific permeability is given by:

$$\frac{P_i^2 - P_o^2}{2P_o L} = \frac{\mu}{k} v \tag{2}$$

where P_i and P_o are the inlet and outlet pressures, respectively. In this work the viscosity of nitrogen gas is taken as 0.0000176 Pa·s at 20°C. From a curve of pressure drop as a function of v the permeability constant k can then be calculated.

3. Results

The key processing and pertinent properties of the mullite-alumina ceramics used in this work are listed in Table I. Fig. 2 shows apparent porosity of mullite-alumina as a function of graphite addition along with the dashed line representing data on pure alumina [7] for comparative

TABLE I Composition, processing parameters and properties of the mullite-alumina ceramics

Material	MA0G	MA20G	MA40G	MA60G
Alumina (wt%)	75 (63 vol%)	75	75	75
Silica (wt%)	25 (37 vol%)	25	25	25
Graphite (vol%)	0	20	40	60
Sintering condition	1540°C, 5 h	1540°C, 5 h	1540°C, 5 h	1540°C, 5 h
Bulk density (g/cm^3)	1.91 ± 0.02	1.82 ± 0.06	1.39 ± 0.07	1.1 ± 0.1
Apparent porosity (%)	43	52	62	71
Average pore size (μm)	6.0 ± 0.3	12.1 ± 1.5	13.8 ± 2.1	22.0 ± 3.5
Pore morphology	Small rounded	Small rounded, large elongated	Small rounded, large elongated	Small rounded, large elongated and irregular
Vickers hardness (GPa)	1.72 ± 0.08	0.47 ± 0.09	0.11 ± 0.01	0.03 ± 0.005

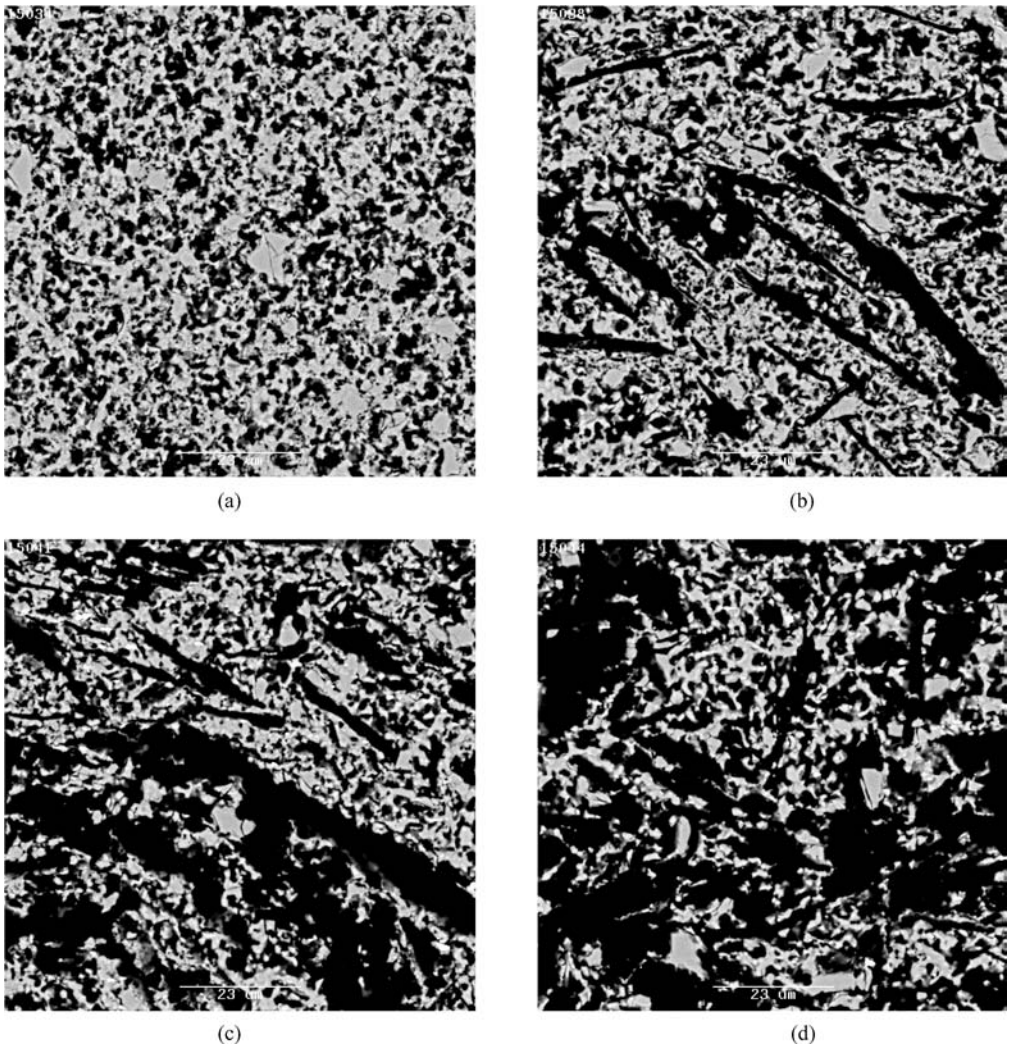

Figure 3 Scanning electron micrographs (backscattered electrons) of the mullite-alumina ceramics: (a) MA0G, (b) MA20G, (c) MA40G and (d) MA60G. The microstructures consist of alumina grains (grey), mullite grains (light) and the dark regions are the pores.

purposes. The pure alumina data presented was produced from the same starting powders used in this work. The porosity data for the mullite-alumina ceramics show that even without pore former, the porosity is about 43% but increased linearly with graphite addition. The high initial porosity of the mullite-alumina material indicates that the reaction-sintering regime used in this work is not optimised and the mullite formed inhibits sinterability [21]. Constrained sintering is also likely, which has been shown to restrict densification of similar ceramic structures [22]. Furthermore it has been shown that the alumina/silica ratio is important with the highest densification rates achieved in systems containing low alumina contents whereas higher alumina compositions (≈75 wt% Al_2O_3) resulted in poor densification [14]. By contrast, the pure alumina data exhibits a strong linear correlation with graphite addition starting from a material with near-zero porosity.

Scanning electron micrographs of polished surfaces in Fig. 3 reveal essential details of the sintered mullite-alumina microstructures. The materials consist of small mullite grains (≈1 μm in size), blocky alumina grains (5 to10 μm in size) and homogeneously distributed pores that vary in size and shape. Without graphite addition the sintered material (Fig. 3a) contains a significant amount of fine porosity (refer to Fig. 2). By contrast the addition of graphite (20 to 60 vol.%) resulted in the formation of large elongated pores along with the small rounded pores (Fig. 3b–d). Grain size was slightly larger for materials with higher porosity, which is probably due to surface diffusion being more dominant. Elemental analysis showed that there was no unreacted silica indicating complete reaction between alumina and silica and this was further confirmed by XRD. Although a small amount of silicate glass (<1%) from any remnant silica reacting with impurities present in the starting alumina powder at temperature could not be ruled out. From analysis of SEM images the average pore size for each material was calculated and these are given in Table I. It is clear from this data that the average pore size in the mullite-alumina structures increases with increasing graphite addition and hence apparent porosity. Fig. 4 depicts the es-

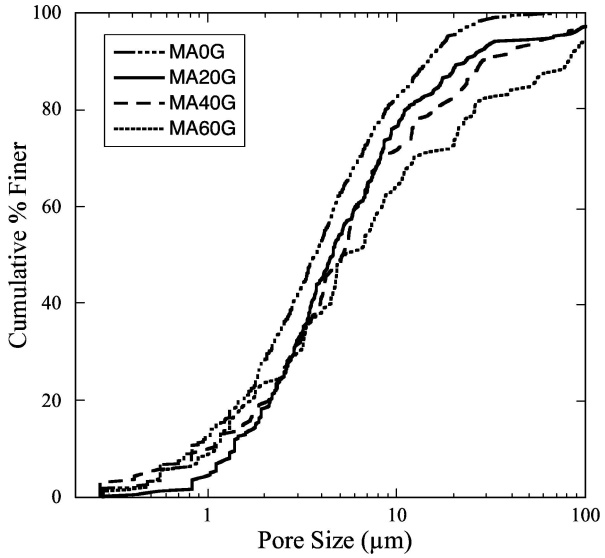

Figure 4 Calculated pore size as a function of cumulative percentage finer for the four materials.

timated pore size as a function of cumulative percentage finer for the four materials based on the SEM image analysis.

The room temperature Young's modulus and biaxial flexure strength of the mullite-alumina ceramics as a function of apparent porosity are shown in Fig. 5. In both instances the data exhibited typical exponential type relations as demonstrated by the exponentially fitted lines, consistent with previous work [7, 15].

Fig. 6 shows in histogram form the room and high temperature biaxial flexure strength data of the mullite-aluminas with four levels of apparent porosity. It is immediately obvious that the strength, irrespective of test temperature, decreases with increasing graphite content (and hence apparent porosity). Moreover, for individual compositions with the same porosity, there is minimal strength degradation at the high temperatures (800 and 1200°C) compared to the room temperature data.

Fig. 7 shows the pressure drop versus gas velocity for the four mullite-aluminas with differing levels of porosity. Solid lines are force fits to the data. From the fitted curves the gas permeability of the porous structures were calculated using Equation 2. The gas permeability versus apparent porosity and average pore size are shown in Fig. 8. As expected, the permeability constant increases with increasing porosity and pore size.

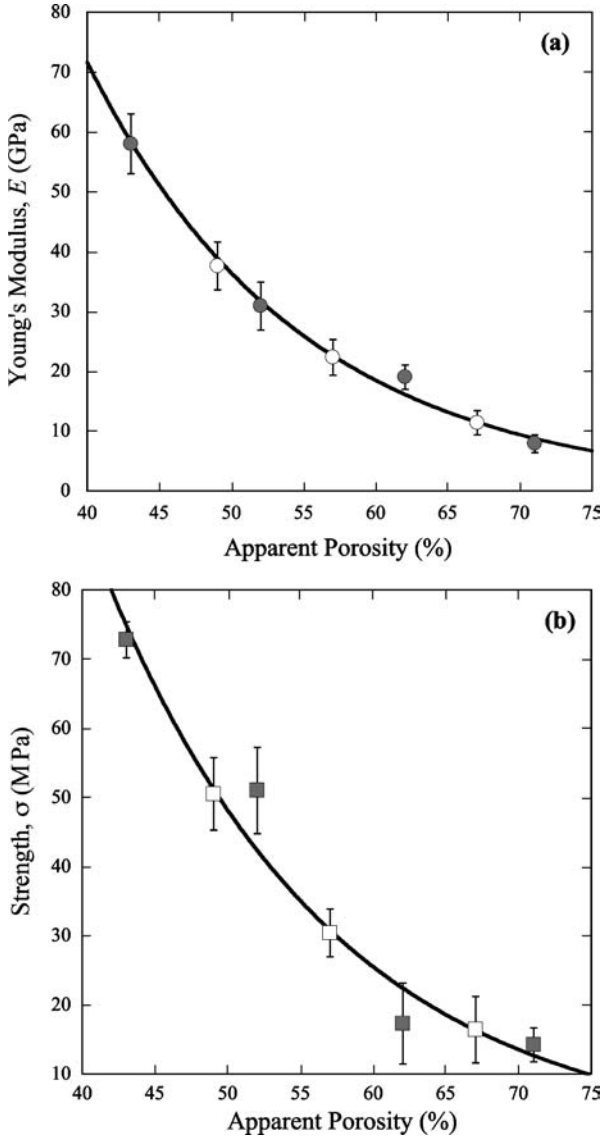

Figure 5 (a) Young's modulus and (b) biaxial flexure strength as a function of apparent porosity for the entire suite of mullite-alumina samples. Data points show means and standard deviations for at least five specimens at each level of porosity. Filled symbols pertain to samples described in Table I. Solid curves are exponential fits to the data.

4. Discussion

In this study we have examined the gas permeability and the room and high temperature strength properties of mullite-alumina ceramics with a range of porosity levels. The mullite-alumina samples were fabricated by reaction sintering and graphite was employed as a fugitive agent to generate residual pores. The level of porosity was controlled by the amount of graphite addition to the starting powders and was found to follow a linear relation (Fig. 2). Furthermore, even without the addition of graphite, the mullite-alumina material has a relatively high porosity (≈43%) and the rate of increase in porosity with graphite is significantly lower compared to that of pure alumina. The high residual porosity indicates that the mullite-alumina system cannot be sintered to full density through reaction sintering with the silica and alumina powders used in this work, signifying that the mullite formed hinders densification. This is quite clearly shown in the micrographs of the materials, with MA0G (Fig. 3a) exhibiting relatively fine rounded pores. Those containing graphite (MA20G, MA40G and MA60G) consisted of a mix of

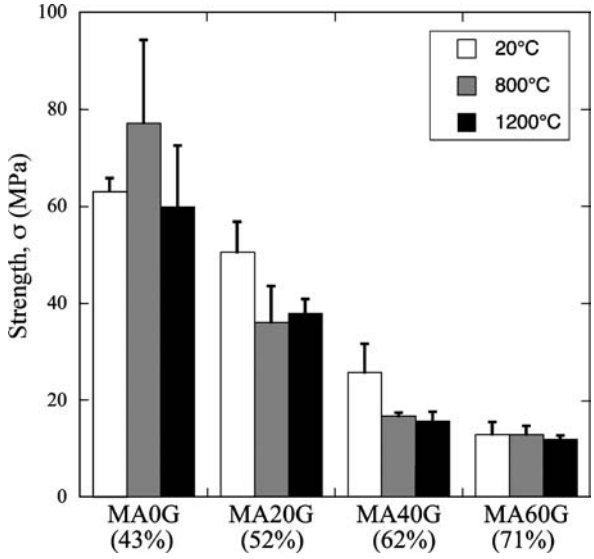

Figure 6 Histogram showing room and high temperature biaxial flexural strengths for the four materials. Error bars indicate standard deviations for five specimens per temperature. Apparent porosities for each material are given in parentheses.

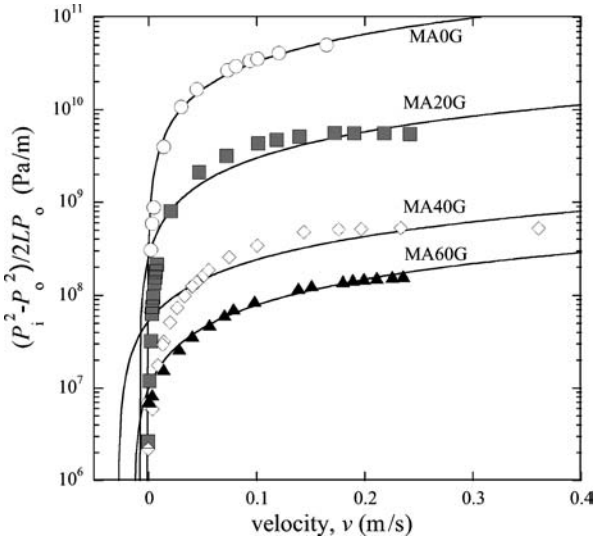

Figure 7 Room temperature nitrogen gas permeability curves for the four materials. Solid curves are force fits to the data.

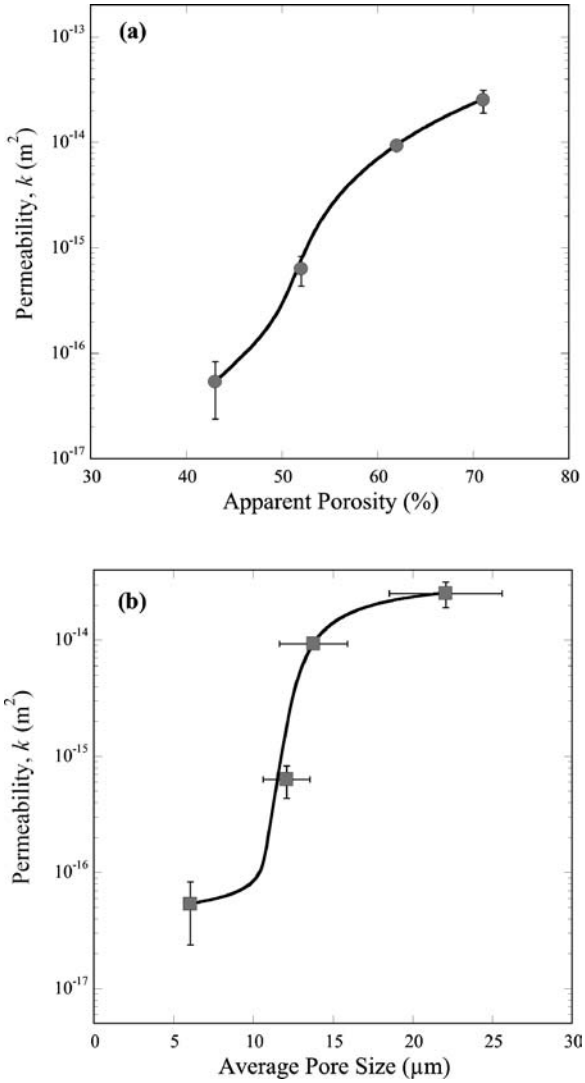

Figure 8 Plots of Darcian permeability constant as a function of (a) apparent porosity and (b) average pore size. Solid curves are empirical fits through the data.

the fine but also large elongated pores that tended to become more irregular in shape due to coalescence of pores for higher graphite additions, as illustrated in Fig. 3b–d. Estimates of the pore sizes from analysis of selected SEM images of each material indicated that the average pore size increased from about 6 μm in MA0G to 22 μm in MA60G.

It is readily apparent from Fig. 5 that the room temperature Young's modulus and biaxial strength versus apparent porosity data of the material follow typical trends and can be expressed empirically using exponential equations, akin to other ceramics [15, 23]. This enables predictions of these properties at specific values of porosity for the mullite-alumina ceramic system. The high temperature strength data for the four key materials at 800 and 1200°C clearly demonstrate that there is no discernible degradation compared to the equivalent room temperature data, although there is a slight strength loss in MA20G and MA40G. In all materials the strength for each porosity level essentially remains constant for the 800 and 1200°C test temperatures. The results confirm that the materials are stable and mechanically reliable at high temperatures for which they are designed. The minimal deterioration in strength at temperature for these porous structures is not surprising given that the equivalent fully dense pure mullite counterparts also exhibit similar behaviour [14]. Intercomparisons of the high temperature strength data of the four materials confirm a typical strength-porosity exponential dependency—commensurate with the ambient temperature data in Fig. 5b. The material with small pores, MA0G, shows greater variabil-

ity in strength response compared to the others indicative of a wide flaw size distribution. This tends to be circumvented particularly in MA40G and MA60G where the flaw population is controlled by the large induced pores. This was confirmed from optical microscopy examinations of failure origin sites of strength test specimens.

From the gas permeability measurements a large pressure differential is discernible for MA0G and this decreases dramatically with addition of graphite (and hence porosity) most notably in MA40G and MA60G. The small pores in MA0G are believed to be the cause of the large pressure drop characteristics compared to the other materials that contain large induced pores. The level of porosity also has a major contribution on the response, with progressively decreasing pressure drop–velocity curves following the sequence MA0G → MA20G → MA40G → MA60G. Interestingly, even through the average pore size of MA20G and MA40G are quite similar, the latter exhibits a lower pressure drop curve.

The specific permeability increases substantially from $k = 5.4\times10^{-17}$ m^2 in MA0G to $k = 2.5\times10^{-14}$ m^2 in MA60G, an increase of approximately 460 times. This is attributable to the combined influence of the porosity fraction and the size and shape of the pores. The gas permeability versus porosity level and pore size data give adequate indications of the general trends in behaviour through which microstructural design can be employed to obtain specific gas permeabilities for these mullite-alumina filters. It is worth noting here that permeability–pore size relations, such as the Kozeny-Carman equation, $k = \varepsilon d^2/32$ (ε is the porosity fraction and d is the pore diameter) [24], can be used to calculate permeability when pore size and porosity is known or alternatively the pore size when permeability and porosity are known. We find that contrary to other studies on similar porous structures [24, 25] the Kozeny-Carman model does not adequately describe our data. From the relation $k/\varepsilon = Ad^n$ (where A and n are constants) and fitting our data with the power law function the following was obtained: $k/\varepsilon = 3.7\times10^{-20}d^{4.53}$ (correlation coefficient, $R = 0.94$). This may be due to certain limitations, namely that the actual permeable porosity may differ markedly to the measured porosity [25] and the average pore size estimated from SEM may differ somewhat to traditional measurements using the bubble-point or mercury intrusion methods.

The data presented in this study provide a good starting point for ascertaining key variables in the processing and fabrication of porous mullite-alumina composites for filter applications. Especially relevant in this context are the gas permeability plots shown in Fig. 8. Selection of a particular gas permeability or range of gas permeabilities for a filter may be chosen from these diagrams enabling fabrication of a suitable structure to meet definite requirements—noting that the two main factors affecting permeability, porosity fraction and pore size, are interconnected. Although, other issues need to be considered such as strength which inevitably requires a degree of compromise in material property requirements. Even so, the MA20G, MA40G and MA60G structures show considerable promise as hot gas filter elements based solely on the high apparent porosities achieved and the reasonable high temperature strengths obtained.

Further work to investigate the influence of a thin denser coating on a porous structural support as described here is underway, given that these thin layers are beneficial in reducing large pressure drops in operation. Moreover, having a denser material is advantageous for improved hardness, contact damage and wear resistance [10]. The long-term strength and stability, thermal shock (see for example [26]) and thermal fatigue behaviour of such porous structures remain to be examined and are important areas for further study.

Acknowledgments

The authors acknowledge Tianshun Liu and Huijin Li for assistance with various aspects of the work.

References

1. L. M. SHEPPARD, *Am. Ceram. Soc. Bull.* **31** (1993) 3.
2. M. A. ALVIN, *Ind. Eng. Chem. Res.* **35** (1996) 3384.
3. J. A. FERNANDO and D. D. L. CHUNG, *J. Porous Mat.* **9** (2002) 211.
4. D. A. HIRSCHFELD, T. K. LI and D. M. LIU, *Key Eng. Mat.* **115** (1996) 65.
5. R. W. RICE, "Porosity of Ceramics and its Effects on Properties" (Marcel Dekker, New York, 1998).
6. J. H. SHE and T. OHJI, *J. Mater. Sci. Lett.* **21** (2002) 1833.
7. H. DENG, B. A. LATELLA, T. LIU, Y. KE and L. ZHANG, *Mat. Sci. Forum* **437–438** (2003) 423.
8. C. C. WU and R. W. RICE, *Ceram. Eng. Sci. Proc.* **6** (1985) 977.
9. B. A. LATELLA, B. H. O'CONNOR, N. P. PADTURE and B. R. LAWN, *J. Am. Ceram. Soc.* **80** (1997) 1027.
10. B. A. LATELLA and B. H. O'CONNOR, *ibid.* **82** (1999) 2145.
11. B. A. LATELLA, *J. Mater. Sci. Lett.* **19** (2000) 1127.
12. C. KANAOKA and M. AMORNKITBAMRUNG, *Powder Tech.* **118** (2001) 113.
13. V. SIBANDA, R. W. GREENWOOD and J. P. K. SEVILLE, *ibid.* **118** (2001) 193.
14. H. SCHNEIDER, K. OKADA and J. PASK, "Mullite and Mullite Ceramics" (John Wiley & Sons, Chichester, 1994).
15. B. A. LATELLA and T. LIU, *J. Aust. Ceram. Soc.* **36** (2000) 13.
16. B. A. LATELLA and S. R. HUMPHRIES, *Scr. Mater.* **51** (2004) 635.
17. ASTM Standards F 394-78, "Standard Test Method for Biaxial Flexure Strength (Modulus of Rupture) of Ceramic Substrates", Annual Book of ASTM Standards, Part 43, Electronics (ASTM, Philadelphia, 1991) p. 313.
18. ASTM Standards C 577-99, "Standard Test Method for Permeability of Refractories", Annual Book of ASTM Standards (ASTM, Philadelphia, 1999) p. 99.
19. A. E. SCHEIDEGGER, "The Physics of Flow Through Porous Media" (University of Toronto Press, Toronto, 1974).
20. E. A. MOREIRA, M. D. M. INNOCENTINI and J. R. COURY, *J. Europ. Ceram. Soc.* **24** (2004) 3209.
21. H. FUJITA, G. JEFFERSON, R. M. MCMEEKING and F. ZOK, *J. Am. Ceram. Soc.* **87** (2004) 261.

22. S.-J. LEE and W. M. KRIVEN, *ibid.* **84** (2001) 767.
23. B. A. LATELLA and T. LIU, *ibid.* **88** (2005) 773.
24. Y. OHZAWA, K. NOMURA and K. SUGIYAMA, *Mater. Sci. Eng.* **A255** (1998) 33.
25. S. DALLAIRE and R. ANGERS, *J. Canadian Ceram. Soc.* **51** (1982) 29.
26. A. BAYUSENO, B. A. LATELLA and B. H. O'CONNOR, *J. Am. Ceram. Soc.* **82** (1999) 819.

Received 23 January
and accepted 31 May 2005